ACERP: Vol. 6, No.2, (Spring 2020) 35-42

Advanced Ceramics Progress

Research Article

Journal Homepage: www.acerp.ir

Synthesis of FAp, Forsterite, and FAp/Forsterite Nanocomposites by Sol-gel Method

S. Manafi [a *], F. Mirjalili [b], S. Joughehdoust [c]

[a] *Department of Materials Engineering, Shahrood Branch, Islamic Azad University, Shahrood, Iran*
[b] *Department of Materials Engineering, Maybod Branch, Islamic Azad University, Maybod, Iran*
[c] *Department of Urology, Maastricht University, The Netherlands*

PAPER INFO

Paper history:

Received 2 June 2020
Accepted in revised form 24 June 2020

Keywords:

Fluorapatite
Forsterite
Nanocomposite
Biomaterials

ABSTRACT

The present study aims to investigate the preparation and evaluation of phase and morphological properties of a nano biocomposite ceramic. In this regard, the synthesis of fluorapatite (FAp) as the first phase and forsterite considered as the second phase by the sol-gel method was taken into account. Then, nanocomposites with the base of fluorapatite with 15, 25, and 35 wt% of forsterite were synthesized using the sol-gel method. The synthesized nanoparticles and nanocomposites were characterized by using different techniques, Field Emission Scanning Electron Microscope (FESEM), X-Ray Powder Diffraction (XRD), and Fourier-Transform Infrared (FT-IR) Spectroscopy. X-ray diffraction test results as well as infrared spectroscopy indicated that fluorapatite, forsterite, and fluorapatite/forsterite nanocomposites were produced without impurity. FESEM result showed that the particle sizes of the produced nanocomposites with 15, 25, and 35 wt% of forsterite ranged approximately between 25 and 80 nm. The result of the MTT assay proved the nontoxicity of samples for 7 days.

1. INTRODUCTION

Bone is a live connective tissue that supplies structural funding to the body organs and is an emergency reservoir of calcium in the correction phase in case of a disease or some pathological processes throughout life [1,2]. Bacterial infection is a severe problem that follows implant surgery in orthopedics and dentistry [3,4]. Numerous studies have pointed out the positive results of bioactive bioceramics regarding bone cell growth [5-6]. The perfect biomaterials for orthopedics may support the mechanical properties and biocompatibility during the period of establishment [7,8]. The agents that demoand hydroxyapatite contain a high degree of decomposition in biological organizations and *in vivo* solubility, which leads to a decrease in use of hydroxyapatite in long-term requests [9-11]. Nevertheless, its biological and physicochemical properties can be strengthened by replacing ions that usually exist in natural bone apatite [10,12].
The inherent brittleness of glass is the major limitation of using bioactive glass as tissue-engineering scaffolds [13,14]. It was discovered that replacing fluoride ions in the hydroxyapatite structure would significantly increase biodegradability. Furthermore, the enhanced absorption of protein expresses a tougher cellular construction and supports the movement of phosphates that create stouter osteoconductivity [15,16]. If OH^- sets in HA are entirely substituted with F^-, fluorapatite [$Ca_{10}(PO_4)_6F_2$] will be prepared [12,17], which has more chemical and structural constancy equated with hydroxyapatite [18-20]. The ion exchange has a positive effect on propagation, morphology, and differentiation of osteoblast-like cells and enhances bioactivity [21,22]. Fluorapatite also forms the external layer of the tooth [19]. The mineral phase of the tooth under the enamel comprises about 0.04-0.07 wt% fluorine [17,23]. The enamel contains fluorapatite with substitution of 50% F^- with OH^- [24].
In 2019, Nguyen and his colleagues established the forsterite bioceramics by using the sol-gel method. Their results designate the adhesion, proliferation, and growth of bone marrow cells on the forsterite ceramic surface. As a result, forsterite ceramic as an ideal bioservice can

* Corresponding Author Email: ali_manafi2005@yahoo.com (S. Manafi)
https://doi.org/10.30501/acp.2020.109549

be appropriate for bone tissue repair. Another research defined biocompatibility of forsterite. In addition, the elasticity of forsterite and its adhesion to dense and spongy bones were among the significant parameters in its collection as biomedical material [25-27].

Forsterite is a magnesium silicate mineral with the chemical formula of $2MgO.SiO_2$. It is a magnesium-rich end-member of the olivine solid solution series with a comparatively high melting point of 1890 °C for refractory demand [27].

Bioactive ceramics have been established in medical demands as a bone substitute material for ruptures. Calcium phosphate ceramics such as hydroxyapatite (HAp: $Ca_{10}(PO_4)_6(OH)_2$) and forsterite are broadly applied as implant materials owing to their biocompatibility with and close semblance to the mineralized phase of human bone structures [1], which can facilitate the formation of new bone with the neighboring tissue [28]. Nanomaterials enjoy an enormously wide range of possible applications from nanoscale optics and electronics to nano-biological systems and nano-medicine. The following methods have been used to synthesize nanosized particles: sol-gel, hydrothermal, solvothermal, sonochemical, direct oxidation, electrodeposition, micelle, and inverse micelle usage, emulsion or hydrolysis precipitation, chemical/physical vapor deposition, microemulsion processes, microwave approaches, and ultrasonic [6-9]. Among the numerous preparation techniques, sol-gel is considered one of the simplest methods for synthesizing nanoparticles in ambient conditions. Besides, it does not require complicated setup and the experimental conditions can be easily controlled [9,11,12]. In addition, sol-gel process can be controlled to obtain the required oxide with a high degree of homogeneity and purity [22].

Likewise, HA and forsterite can be made from natural sources with calcium-based structures such as bovine bone, mollusk shell, or corals [29]. Consequently, these materials may be considered as cost-effective biomaterials for bone tissue engineering in bone graft applications. HA is presently used as implant material in orthopedic surgery and dental implant due to its biocompatibility, osteoconductivity, and chemical similarity to the human skeletal system [5]. It has a calcium-to-phosphate ratio of 1.67, which is homologous to natural human bone [26]. Conversely, bulk HA cannot be used as load-bearing implants due to low mechanical properties such as great brittleness [27]. To this end, investigators have previously attempted to combine HA with forsterite to develop composite biomaterials structure with enhanced mechanical and biological properties [28]. This grouping may be attained through sintering; however, sintering above 597 °C would source forsterite crystallization [29]. The $Na_2Ca_2Si_3O_9$ crystalline phase formed recovers the mechanical property [29] and bioactive response [26].

The combination of fluorapatite particles with forsterite affords its special properties such as augmentation of bioactivity and mechanical properties.

The present study aims to synthesize and characterize fluorapatite, forsterite, and fluorapatite/forsterite nanocomposite by the sol-gel method for bone tissues. The novelties of this research are exploring the effect of different percentages of forsterite for preparing the fluorapatite-forsterite nanocomposite, investigationg the morphological and microstructure properties of fluorapatite-forsterite nanocomposites and fluorapatite, and considering forsterite nanoparticles.

The present study aims to develop and evaluate a ceramic nanosized composite with properties close to bone properties and good biocompatibility for dentistry and orthopedics applications as a bone constructor.

2. EXPERIMENTAL PROCEDURES

2.1. Preparation of FAp Powder

First, 5.91 g hydrated calcium nitrate ($Ca(NO_3).4H_2O$, 98%, Merck, CN)) was dissolved in 20 ml absolute (98%, Merck, ET)/water (W) and then, another solution was made by dissolving 1.36 g triethyl phosphate (97%, Merck, EP) in 20 ml ET/W. Then, 0.28 g fluoride ammonium (97%, Merck, FAp) was dissolved in 20 ml (ET)/W. Three solutions were stirred to obtain transparency for 24 h. At the second step, the calcium solution was added dropwise at a rate of 5 ml/min to phosphate solution with vigorous stirring for 72 h. A milky and gelatinous precipitate was obtained. The obtained precipitates were centrifuged and washed by ethanol four times, dried at 80 ºC for 5 h, and subsequently ground with mortar and pestle. Finally, the resulting fine fluorapatite powders were heated to 550 °C for 1 h.

2.2. Preparation of Forsterite

In order to prepare forsterite (FO), aqueous magnesium nitrate (98%, Merck, MN) solution was prepared in 50 cc distilled water. After the dissolution of magnesium nitrate in distilled water on a magnetic stirrer, colloidal silicon oxide with the molar ratio of magnesium to silicon 2:1=Si: Mg was added and the magnetic stirrer was homogenized. The required amount of sucrose was dissolved in 100 cc of distilled water and added to the mentioned solution. After 2 h of homogenization at ambient temperature, polyvinyl alcohol (Merck, 96%, PVA) solution was distilled in 20 cc of water with magnesium to polyvinyl alcohol ratio of 0.8 and added to the mentioned solution. The pH was adjusted to 1. To uniformly distribute the raw materials and accelerate the

hydrolysis process, the above solution was stirred by a magnetic stirrer for 2 h at ambient temperature of 80 °C. Subsequently, to complete the hydrolysis and polymerization processes of the precursors and to ensure sufficient time for the ions to be uniformly distributed in the structure, aging operations were carried out at ambient temperature for 24 h and dried at 100 °C and sintered at 900 °C for 2 h.

2.3. Preparation of Fap/Forsterite Nanocomposite

To synthesize FAp/forsterite nanocomposites with 15, 25, and 35% wt% of forsterite, three sols were prepared. First, 5.91 g of calcium nitrate of tetrahydrate ($Ca(NO_3)_2.4H_2O$, 98%, Merck, CN) in 20 ml absolute ET/W solution (75% -25%) was dissolved. Then, 1.365 g triethyl phosphate (99%, Merck, TP) in 20 ml absolute ET / W (75%-25%) was stirred for 1 h. In the meantime, 0.28 g ammonium fluoride (99%, Merck, AF) was dissolved in 20 ml absolute ET/W (75-25%) and stirred at 45 °C. Finally, forsterite powder with 15, 25, and 35wt% was added to the final solution and stirred for 48 h. Furthermore, the solutions were dried for 24 h at 110 °C and sintered at 600 °C for 2 h. The sample names are shown in Table 1.

TABLE 1. The name of the samples

Code	Sample
FAp	Fluorapatite of 100%
FAp-F-15	Fluorapatite-Forsterite of 15%
FA-F-25	Fluorapatite-Forsterite of 25%
FA-F-35	Fluorapatite-Forsterite of 35%
FO	Forsterite of 100%

2.4.Characterization of FAp/Forsterite Nanocomposite

Phase identification was performed by X-Ray Diffraction (XRD) PW1800, of Philips Company, using nickel-filtered CuK_α radiation in the range of 2θ=10-60° at a scanning speed of 5° per minute. A Perkin Elmer Spectrum 100 series Fourier FT-IR (Transform Infrared Spectrometer) was used in conjunction with the Universal Attenuated Total Reflection (UATR) method. Microstructures of powders were identified by transmission electron microscope (Philips–Zeiss-Germany), Scanning Electron Microscopy (SEM PHENOM), and field Emission Scanning Electron Microscope (FESEM).

2.5. Evaluation of Cell Survival By MTT Test

At the next step, the proliferation and survival of L929 cells on the surface of the samples were evaluated by MTT assay. To prepare the samples, a common protocol for this test was used. In this way, 5 mg of each sample was mixed in the medium and incubated at 37 °C for 7 days. The stored stock of MTT solution was added to the control and the treated cell line samples and again incubated at 37 °C for 3 h. Then, the medium was removed and mixed with solubilizing buffer. During this process, the MTT ring was broken, thus creating crystalline purplish color. The intensity of this color was directly related to the living cells. Next, the supernatant was discarded and the cells were washed. Finally, the absorbance of the solution was calculated by the spectrophotometer. The following formula was then used to determine the survival rate:

Cell Viability% = ODs/ODc

ODs Optical Density Sample, ODc Optical Density Control.

3. RESULTS AND DISSCUSSION

3.1. X-Raydiffraction Analysis of Forsterite, FAp, FAp/Forsterite Nanocomposite

Fig. 1(a) shows the XRD patterns of the forsterite powder. Based on the X-ray diffraction pattern, it represents a broad and longer form expressing the amorphous structure of the synthesized nanopowder. The peaks belonging to the crystalline phases are visible at angles of 22.81, 23.89, 29.53, 44.57, 64.94, and 65.59°, depending on the effects of crystalline phases of forsterite (JCPDS No. 00-004-0769).

X-ray diffraction pattern of nano-powdered synthetic FA is shown in Fig. 1(b). It was discovered that all the peaks identified in the diffraction pattern were related to the structure of fluorapatite with JCPDS No.00-003-0736 with a hexagonal crystal structure. The peaks belonging to the crystalline phases were visible at angles of 21.78, 25.77, 28.99, 48.19, 60.13, and 63.07°. Based on interpretation of the diffraction pattern, it can be concluded that this structure is well crystallined.

Figs. 1(c-e) show the X-ray diffraction pattern of the FAp/forsterite nanocomposites. The synthetic nanosized particles were distinguishable from the synthesized composite dispersion pattern. Based on the examined patterns, it can be conluded that these patterns are very difficult to be distinguished due to the overlapping of the peak of the forsterite with apatite peaks.

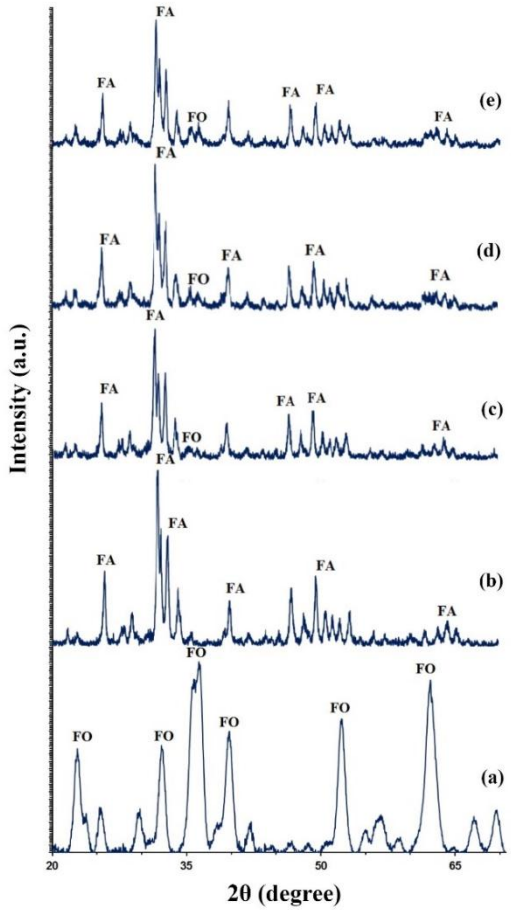

Figure 1. X-ray diffraction pattern of a) nano-powdered synthetic FO; b) nano-powdered synthetic FAp; c) FAp-F-15 nanocomposite; d) FAp-F-25 nanocomposite; e) FAp-F-35 nanocomposite

However, the most significant peak of forsterite, the one at 2θ=36.53°, was detectable in all patterns due to lack of overlap with the fluorapatite peaks; in addition, its intensity increased as the forsterite weight percentage increases. Mazrooei Sebdani et al. discovered that the crystallite size increased by enhancing the Forsterite phase in hydroxyapatite–forsterite–bioactive glass nanocomposite coatings [30]. In another research, Forghani et al. found no grain growth during calcination in Fluorapatite- Forsterite Nanocomposite [31]. However, no significant changes in the crystallinity in XRD peaks were detected in this study.

3.2. Infradspectroscopy Analysis of Forsterite, FAp, FAp/Forsterite Nanocomposite

Forsterite characteristic bands mainly consist of two main categories: one visible peak at 890-1090 cm^{-1}, 841 cm^{-1}, and 614 cm^{-1} corresponding to SiO_4 group vibrational modes, and the other two peaks at 425 cm^{-1} and 2510 cm^{-1} regarded as vibrational modes of octahedral of MgO [27,28].

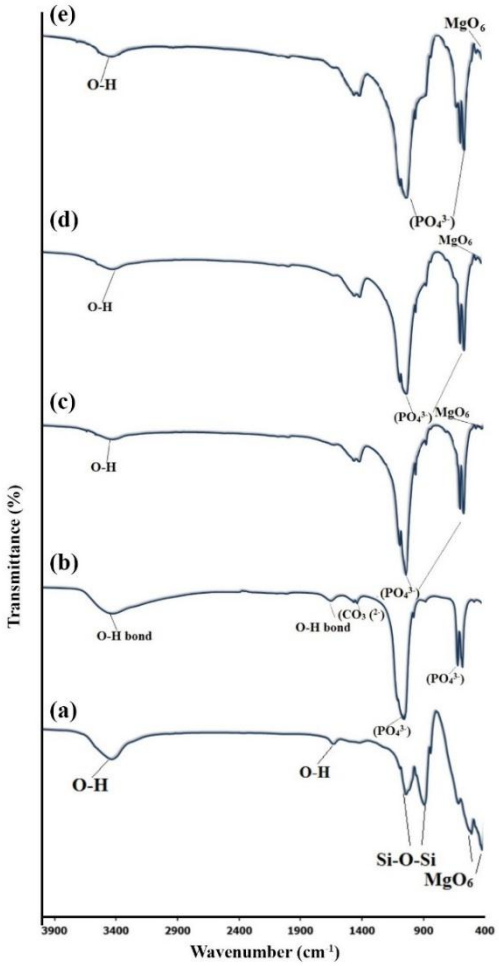

Figure 2. Infrared spectroscopy analysis of a) nano-powdered synthetic FO; b) nano-powdered synthetic FAp; c) FAp-F-15 nanocomposite; d) FAp-F-25 nanocomposite; e) FAp-F-35 nanocomposite

In the FTIR spectrum of pure forsterite, the peaks at 1634 cm^{-1} and 3433 cm^{-1} corresponded to the bending vibrations of water molecules adsorbed on the surface of nanoparticles and tensile vibrations of the O-H group in the water molecule. The peak at 1044 cm^{-1} was due to the tensile vibrations of Si-O-Si bonds in the silicate lattice in the forsterite [29]. Except for the characteristic peaks mentioned, no other peaks related to the structural impurities in the spectrum could be observed, which might confirm the structural purity of the synthesized sample (Fig. 2(a)).

Fig. 2(b) shows the FTIR spectrum of the synthesized fluorapatite nanoparticles. The relevant FTIR spectrum

had all vibrations from v_4 to v_1 related to the phosphate group in the structure of apatite [16]. Finally, there were two courier sharps of 564 cm^{-1} and 603 cm^{-1} belonging to the group of v_4 vibrations [17]. The presented peak at 741 cm^{-1} represented the hydroxyl chain, which was found in this structure that was rich in fluorine [21]. The peaks at 1640 cm^{-1} and 3700 cm^{-1} were related to O-H groups. A central peak of 873 cm^{-1} along with a band with two edges of 1413 cm^{-1} and 1465 cm^{-1} were attributed to structural carbonate (CO_3^{2-}) groups [19]. The presence of this group proved the bioavailability of fluorapatite.

FTIR spectra of fluorapatite-forsterite composites with 15, 25, and 35 wt% of forsterite contained absorption peaks corresponding to each component (Figs. 2(c-e)). As shown, the FTIR curve of nanocomposites did not significantly change by adding different percentages of forsterite. However, the intensities of the forsterite characteristic peaks, especially the peaks at 510 cm^{-1}, 890 cm^{-1}, and 1040 cm^{-1}, gradually increased as the weight percentage of the forsterite in the composite samples increased.

3.3. Morphological Properties of Forsterite, FAp, FAp/Forsterite Nanocomposite

Field Emission Scanning Electron Microscopy (FESEM) images of fluorapatite, forsterite, and fluorapatite/forsterite nanocomposites with different forsterite percentages are presented in Figs. 3 and 5. Fig. 3(a) depicts the FESEM images of synthesized forsterite. It can be noted that the nanoparticle is characterized by spherical morphology with some agglomeration due to the intrinsic nature of nanoparticles, and their particle size ranged from 48 to 25 nm. Fig. 3(b) shows the FESEM microsphere of the synthesized fluorapatite nanoparticles. In addition, the formation of nanometric particles with spherical morphology and a particle size range of 23-30 nm are given.

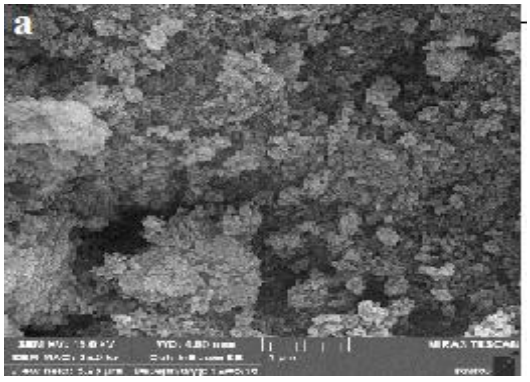

(a)

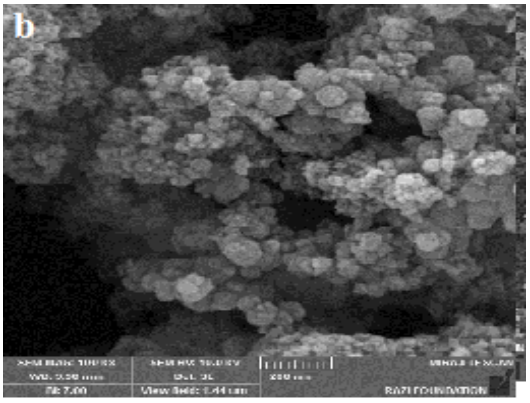

(b)

Figure 3. Field emission scanning images of a) FO, b) FAp

According to Fig. 4(a), the EDS pattern of the synthesized FO particles showed the major constituent elements, namely silicon, magnesium, and oxygen, at the atomic ratio close to the stoichiometric sample of Mg_2SiO_4. The pattern showed no impurity, indicating the high elemental purity of the synthetic forsterite particles. According to Fig. 4(b), the EDS pattern of the fluorapatite nanoparticles indicated that the nanoparticles were composed of four dominant elements: calcium, phosphorus, fluorine, and oxygen, which were essentially the constituent elements of fluorapatite according to the experimental $Ca_5(PO_4)_3F$ formula. The EDS pattern did not show the peaks characteristic of other impurities, which could be considered as a good criterion for the high elemental purity of the synthesized nanoparticles.

FESEM images of FAp/forsterite nanocomposites with different forsterite percentages are presented in Figs. 5(a-c). As shown earlier, the spherical shape of these synthesized particles with different particle sizes ranging from about 20 nm to 80 nm in three samples confirmed the XRD results. The particle sizes of FA-F-15 ranged from 45 to 80 nm. Moreover, as the forsterite particles increased, the particle sizes became finer in FA-F-25 and FA-F-35. The particle sizes in FA-F-25 ranging from 33-45 nm reached 20-40 nm in FA-F-35.

Moreover, as the Forstrite particles increase, the particle sizes become finer. This outcome was predictable due to the different diffusivity rates of between silicon and magnesium and the greater number of fluorapatite-fluorapatite grain boundaries made the growth of forsterite harder [2]. Apatite containing phase-forsterite with emphasis on SiO_2 and MgO showed slow diffusivity and exiguous presence in the assembly. These findings were also the result of research by Hiraga and Johanson who worked on synthesis and grain growth of Periclase as the main phase and forsterite as the second phase. The EDS pattern in Fig. 6 shows the

presence of oxygen, fluorine, magnesium, silicon, phosphorus, and calcium, which were the main constituents of the two structural components of the nanocomposite without the presence of impure elements.

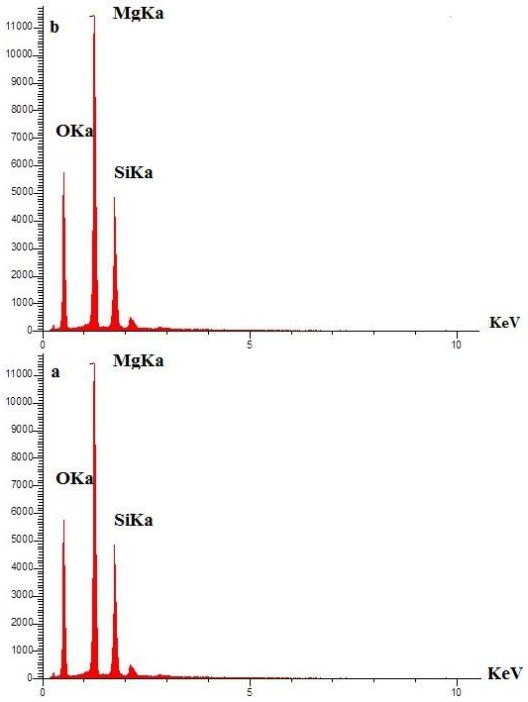

Figure 4. EDX of a) FO nanoparticle, b) EDX of FAp nanoparticle

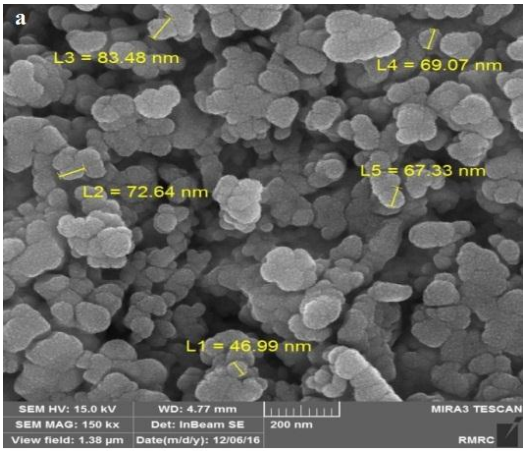

(a)

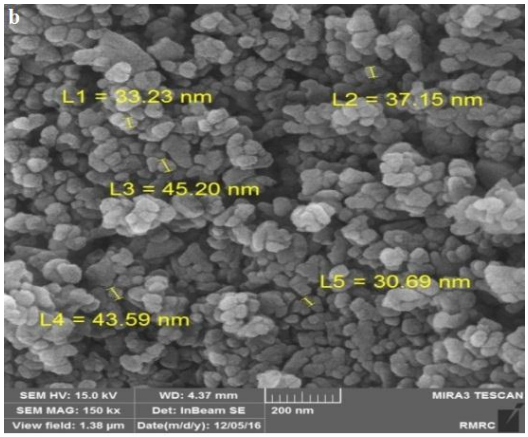

(b)

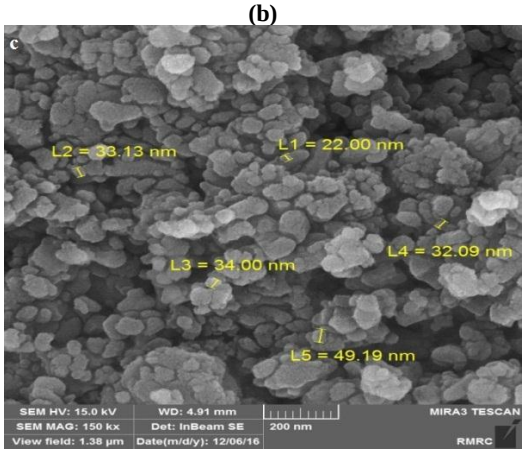

(c)

Figure 5. Field emission scanning images of FAp/forsterite nanocomposites a) FAp-F-15, b) FAp-F-25, and c) FA-F-35

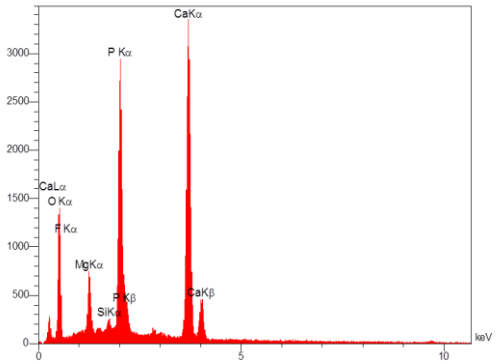

Figure 6. EDX pattern of FAp-F-25 nanocomposite

3.4. MTT TEST

The results of the MTT test (3-(4,5-dimethylthiazol-2-yl)-2,5-diphenyltetrazolium bromide) after 7 days are presented in Fig. 7. Regarding the shape, it can be found that by increasing the time duration of cell replacement

with the extract in all three main samples, negative control and positive control of cellular responses increased by 15 and 25% of forsterite, but the probability of cell survival was reduced with a 35% forsterite increase.

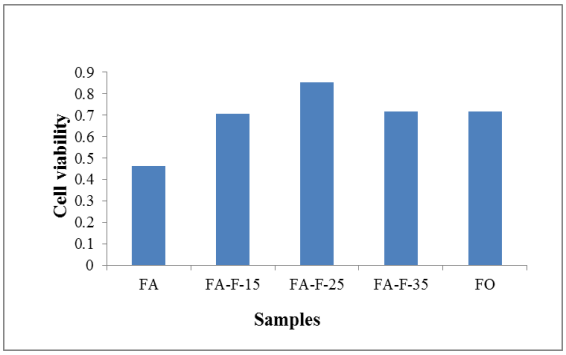

Figure 7. MTT cell survival test for all the samples after 7 days

TABLE 2. The results of the MTT cell survival test for all materials after 7 days

OD 7 days	Mean	SE
FA	0.382	0.031
FO	0.216	0.029
FA-F-35	0.292	0.024
FA-F-25	0.593	0.041
FA-F-15	0.479	0.031
Control	0.59	0.0223

Based on a comparison of the results, the FA-F-25 showed better behavior than FA-F-15 and FA-F-35, which related to the equilibrium recognized in this type of composite in terms of ion release and subsequent relative toxicity.

4. CONCLUSION

Nano forsterite and nano fluorapatite were prepared by the modified sol-gel method, and nano fluorapatite/forsterite nanocomposite with 15%, 25%, and 35% of forsterite was prepared by the modified sol-gel method at 600 °C with particle sizes ranging between 20-80 nm. Based on the X-ray diffraction patterns of forsterite and fluorapatite, the crystalline phases of forsterite with JCPDS No. 00-004-0769 and fluorapatite with JCPDS No. 00-003-0736 with a hexagonal crystal structure were produced, respectively. FTIR analysis indicated that fluorapatite and forsterite without impurities were produced. Also, the FTIR curve of nanocomposites did not change clearly by adding different percentages of forsterite. FESEM images of fluorapatite, forsterite, and fluorapatite/forsterite nanocomposites with different forsterite percentages showed the spherical shape of these synthesized particles with different particle sizes in all samples. The particle sizes of FA-F-15 ranged between 45-80 nm. Moreover, as the forsterite particles increased, the particle sizes became finer in FA-F-25 and FA-F-35. The results of the MTT cell survival test for all materials after 7 days did not show any toxicity.

REFERENCES

1. Manafi, S., Joughehdoust, S., "Synthesis and in vitro investigation of sol-gel derived bioglass-58S nanopowders", ***Materials Science-Poland***, Vol. 30, (2012), 45–52. DOI:10.2478/s13536-012-0007-2
2. Hiraga, T., Miyazaki, T., Tasaka, M., Yoshida, H., "Mantle Superplasticity and Self-made Demise", ***Nature***, Vol. 468, (2010), 1091–1094. DOI:10.1038/nature09685
3. Johnson, C.H., Richter, S.K., Hamilton, C.H., Hoyt, J.J., "Static Grain Growth in a Microduplex Ti-6Al-4V alloy", ***Acta Materialia***, Vol. 47, (1998), 23–29. DOI:10.1016/S1359-6454(98)00341-3
4. Sun, Y., Yang, H., Tao, D., "Microemulsion Process Synthesis of lanthanide-doped Hydroxyapatite Nanoparticles under Hydrothermal Treatment", ***Ceramics International***, Vol. 37, (2011), 2917-2920. DOI:10.1016/j.ceramint.2011.03.030
5. Sumathi, S., Gopal, B., "In Vitro Degradation of Multisubstituted Hydroxyapatite and Fluorapatite in the Physiological Condition", ***Journal of Crystal Growth***, Vol. 422, (2015), 36-43. DOI:10.1016/j.jcrysgro.2015.04.022
6. Choudhary, R., Chatterjee, A., Venkatraman, S., Koppala, S., Abraham, J., "Antibacterial forsterite (Mg_2SiO_4) scaffold: A promising bioceramic for load bearing applications", ***Bioactive Materials***, Vol. 3, (2018), 218-224. DOI:10.1016/j.bioactmat.2018.03.003
7. Basar, B., Tezcaner, A., Keskin, D., Evis, Z., Improvements in Microstructural, Mechanical, and Biocompatibility Properties of nano-sized Hydroxyapatites Doped with Yttrium and Fluoride, ***Ceramics International***, Vol. 36, (2010), 1633-1643. DOI:10.1016/j.ceramint.2010.02.033
8. Kheradmandfard, M., Fathi, M., "Preparation and Characterization of Mg-doped Fluorapatite Nanopowders by Sol-Gel Method", ***Journal of Alloys and Compounds***, Vol. 504, (2010), 141-145. DOI:10.1016/j.jallcom.2010.05.073
9. Mancuso, E., Bretcanu, O., Marshall, M., Dalgarno, K.W., "Sensitivity of Novel Silicate and Borate-Based Glass Structures on In vitro Bioactivity and Degradation Behaviour", ***Ceramics International***, Vol. 43, (2017), 12651-12657. DOI:10.1016/j.ceramint.2017.06.146
10. Chen, W., Wang, Q., Meng, S., Yang, P., Jiang, L., Zou, X., Li, Z., Hu, S., "Temperature-Related Changes of Ca and P Release in Synthesized Hydroxylapatite, Geological Fluorapatite, and Bone Bioapatite", ***Chemical Geology***, Vol. 451, (2017), 183-188. DOI:10.1016/j.chemgeo.2017.01.014
11. Barandehfard, F., Rad, M.K., Hosseinnia, A., Khoshroo, K., Tahriri, M., Jazayeri, H.E., Moharamzadeh, K., Tayebi, L., "The Addition of Synthesized Hydroxyapatite and Fluorapatite Nanoparticles to a Glass-Ionomer Cement for Dental Restoration and its Effects on Mechanical Properties", ***Ceramics***

International, Vol. 42, (2016), 17866-17875. DOI:10.1016/j.ceramint.2016.08.122

12. Santos, S.C., Barreto, L.S., dos Santos, E.A., "Nanocrystalline Apatite Formation on Bioactive Glass in a Sol-Gel Synthesis", ***Journal of Non-Crystalline Solids***, Vol 439, (2016), 30-37. DOI:10.1016/j.jnoncrysol.2016.02.013
13. Shen, J., Jin, B., Jian, Q. Y., Hu, Y. M., Wang, X. Y., "Morphology-Controlled Synthesis of Fluorapatite Nano/Microstructures via Surfactant-Assisted Hydrothermal Process", ***Materials & Design***, Vol. 97, (2016), 204-212. DOI:10.1016/j.matdes.2016.02.091
14. Sumathi, S., Gopal, B., "In vitro Degradation of Multisubstituted Hydroxyapatite and Fluorapatite in the Physiological Condition", ***Journal of Crystal Growth***, Vol. 422, (2015), 36-43. DOI:10.1016/j.jcrysgro.2015.04.022
15. Roche, K. J., Stanton, K. T., "Measurement of Fluoride Substitution in Precipitated Fluorhydroxyapatite Nanoparticles", ***Journal of Fluorine Chemistry***, Vol. 161, (2014), 102-109. DOI:10.1016/j.jfluchem.2014.02.007
16. Zhao, J., Dong, X., Bian, M., Zhao, J., Zhang, Y., Sun, Y., Chen, J., Wang, X., "Solution Combustion Method for Synthesis of Nanostructured Hydroxyapatite, Fluorapatite and Chlorapatite", ***Applied Surface Science***, Vol. 314, (2014) 1026-1033. DOI:10.1016/j.apsusc.2014.06.075
17. Tredwin, C. J., Georgiou, G., Kim, H. W., Knowles, J. C., "Hydroxyapatite, Fluor-hydroxyapatite, and Fluorapatite Produced via the Sol-Gel Method: Bonding to Titanium and Scanning Electron Microscopy", ***Dental Materials***, (2013), 521-529. DOI:10.1016/j.dental.2013.02.002
18. Nasiri-Tabrizi, B., Fahami, A., "Synthesis and Characterization of Fluorapatite–Zirconia Composite Nanopowders", ***Ceramics International***, Vol. 39, (2013), 4329-4337. DOI:10.1016/j.ceramint.2012.11.016
19. Joughehdoust, S., Behnamghader, A., Jahandideh, R., Manafi, S., "Effect of Aging Temperature on Formation of Sol-Gel Derived Fluor-Hydroxyapatite Nanoparticles", ***Journal of nanoscience and nanotechnology***, Vol. 10, (2010), 2892-2896. DOI:10.1166/jnn.2010.1397
20. Cooper, L.F., Zhou, Y., Takebe, J., Guo, J., Abron, A., Holmén, A., Ellingsen, J.E., "Fluoride Modification Effects on Osteoblast Behavior and Bone Formation at TiO_2 Grit-blasted CP Titanium Endosseous Implants", ***Biomaterials***, Vol. 27, (2006), 926-936. DOI:10.1016/j.biomaterials.2005.07.009
21. Rodrıguez-Lorenzo, L., Hart, J., Gross, K., "Influence of Fluorine in the Synthesis of Apatites. Synthesis of Solid Solutions of Hydroxy-Fluorapatite", ***Biomaterials***, Vol. 24, (2003), 3777-3785. DOI:10.1016/S0142-9612(03)00259-X
22. Loher, S., Stark, W.J., Maciejewski, M., Baiker, A., Pratsinis, S.E., Reichardt, D., Maspero, F., Krumeich, F. and Günther, D., "Fluoroapatite and Calcium Phosphate Nanoparticles by Flame Synthesis", ***Chemistry of Materials***, Vol. 17, (2005), 36-42. DOI:10.1021/cm048776c
23. Rey, C., Combes, C., Drouet, C., Sfihi, H., "Fluoride-based Bioceramics" In ***Fluorine and Health: Molecular Imaging, Biomedical Materials and Pharmaceuticals***, Amsterdam: Elsevier, (2008), 279-331. DOI:10.1016/B978-0-444-53086-8.00006-0
24. Chitsazi, M.T., Shirmohammadi, A., Faramarzie, M., Pourabbas, R., Rostamzadeh, A.N., "A Clinical Comparison of Nano-Crystalline Hydroxyapatite (Ostim) and Autogenous Bone Graft in the Treatment of Periodontal Intrabony Defects", ***Medicina Oral Patologia Oral y Cirugia Bucal***, Vol. 16, (2011), 448-453. DOI:10.4317/medoral.16.e448
25. Nguyen, M., Sokolar, R., "Presence of Magnesium-Alumina Spinel in Forsterite Ceramics and its Influence During Sintering and on Resulting Properties of Fired body", ***IOP Conference Series: Materials Science and Engineering***, Czech Republic, Vol. 549, (June. 1, 2019), 2019. DOI:10.1088/1757-899X/549/1/012025
26. Wassanai, W., Jidapah, R., Pana, S., "Appropriate Forming Conditions for Hydroxyapatite-Bioactive Glass Compact Scaffold", ***Engineering Journal***, Vol. 20, (2016), 123-134. DOI:10.4186/ej.2016.20.3.123
27. Ni, S., Chou, L ., "Preparation and Characterization of Forsterite (Mg, SiO_4) Bioceramics", ***Ceramics International***, Vol. 33, (2007), 83-88. DOI:10.1016/j.ceramint.2005.07.021
28. Chin, K. M., Lee, K. Y., Tan, C. Y., Singh, R., Teng, W. D., "Characterization of Forsterite Synthesized by Solid-State Reaction with Ball Milling Method", ***Applied Mechanics and Materials***, Vol. 372, (2013), 416-419. DOI:10.4028/www.scientific.net/AMM.372.416
29. Petric, N., Martinac, V., Tkalcec, E., Ivankovic, V., Petric, B., "Thermodynamic Analysis of Results Obtained by Examination of the Forsterite and Spinel Formation Reactions in the Process of Magnesium Oxide Sintering", ***Industrial & Engineering Chemistry Research***, Vol. 28, (1989), 298–302. DOI:10.1021/ie00087a008
30. Mazrooei Sebdani, M., Fathi, M. H., "Preparation and characterization of hydroxyapatite–forsterite–bioactive glass nanocomposite coatings for biomedical applications", ***Ceramics International***, Vol. 38, (2012), 1325-1330. DOI:10.1016/j.ceramint.2011.09.008
31. Forghani, A., Mapar, M., Kharaziha, M., Fathi, M. H., Fesharaki, M., "Novel Fluorapatite- Forsterite Nanocomposite Powder for Oral Bone Defects", ***International Journal of Applied Ceramic Technology***, Vol. 10, (2012), E282-E289. DOI:10.1111/j.1744-7402.2012.02824.x